Speed limits of the laser-induced phase transition in FeRh

Cite as: APL Mater. 12, 051124 (2024); doi: 10.1063/5.0206095
Submitted: 29 February 2024 • Accepted: 7 May 2024 •
Published Online: 28 May 2024

M. Mattern,[1] J. Jarecki,[1] J. A. Arregi,[2] V. Uhlíř,[2,3] M. Rössle,[4] and M. Bargheer[1,4,a)]

AFFILIATIONS

[1]Institut für Physik und Astronomie, Universität Potsdam, 14476 Potsdam, Germany
[2]CEITEC BUT, Brno University of Technology, 61200 Brno, Czech Republic
[3]Institute of Physical Engineering, Brno University of Technology, 61669 Brno, Czech Republic
[4]Helmholtz-Zentrum Berlin für Materialien und Energie GmbH, Wilhelm-Conrad-Röntgen Campus, BESSY II, 12489 Berlin, Germany

Note: This paper is part of the Special Topic on Ultrafast Materials Science: Coherence and Dynamics.
[a)]**Author to whom correspondence should be addressed:** bargheer@uni-potsdam.de

ABSTRACT

We use ultrafast x-ray diffraction and the polar time-resolved magneto-optical Kerr effect to study the laser-induced metamagnetic phase transition in two FeRh films with thicknesses below and above the optical penetration depth. In the thin film, we identify an intrinsic timescale for the light-induced nucleation of ferromagnetic (FM) domains in the antiferromagnetic material of 8ps, which is substantially longer than the time it takes for strain waves to traverse the film. For the inhomogeneously excited thicker film, only the optically excited near-surface part transforms within 8ps. For strong excitations, we observe an additional slow rise of the FM phase, which we experimentally relate to a growth of the FM phase into the depth of the layer by comparing the transient magnetization in frontside and backside excitation geometry. In the lower lying parts of the film, which are only excited via near-equilibrium heat transport, the FM phase emerges significantly slower than 8ps after heating above the transition temperature.

First-order phase transitions are characterized by an abrupt change of structural, electronic, or/and magnetic properties and a co-existence of multiple phases that introduces nucleation and domain growth to the kinetics of the phase transition.[1–10]

The abrupt change of properties accompanying the emerging phase as a consequence of a fine interplay of spin, charge, orbital, and lattice degrees of freedom[6,11] predestine materials featuring first-order phase transitions for ultrafast laser control of functionalities.[12] In this context, the first-order antiferromagnetic to ferromagnetic (AFM-FM) phase transition of FeRh at 370K attracted considerable attention in terms of ultrafast generation of ferromagnetic order[13,14] that extends the more extensively studied ultrafast demagnetization[15,16] and magnetization reversal.[17–19]

The metamagnetic phase transition in FeRh is parameterized by the expansion of the unit cell,[20] the change in the electronic band structure,[21,22] and the arising magnetization,[23,24] which each serve as order parameters for different aspects of the ultrafast laser-induced phase transition. Time-resolved photoelectron spectroscopy experiments reveal the formation of an electronic signature of the ferromagnetic state by a photo-induced change of the band structure on a sub-picosecond timescale.[25] X-ray magnetic circular dichroism,[26,27] magneto-optical Kerr effect (MOKE),[28] and double-pulse THz emission spectroscopy[29] report a subsequent formation of an in-plane magnetization on a 100 ps timescale. While the rise of a macroscopic magnetization is dominated by the slow coalescence and alignment of the nucleated domains in an external magnetic field,[14,29] the large FM lattice constant as a structural order parameter is independent of the orientation of the arising magnetization.[28] Hence, ultrafast x-ray diffraction (UXRD) directly accesses the nucleation and growth of FM domains, which also determines the rise of the laser-induced magnetization within the first picoseconds.[28,29] Previous UXRD studies report nucleation timescales ranging from 15 to

90 ps, depending on the probing depth and fluence.[28,30] Thus, the kinetics of the nucleation and growth of the laser-induced FM phase remains unclear and controversial.

Here, we use UXRD experiments on a homogeneously optically excited 12 nm thin FeRh film to identify an intrinsic fluence-, temperature-, and field-independent 8 ps rise time of the structural order parameter. This nucleation of the FM phase is not limited by the time that it takes for strain waves to traverse the film at the speed of sound, which requires only 2.5 ps. For the inhomogeneously excited 44 nm thick film, we observe the same intrinsic 8 ps nucleation timescale and an additional delayed slow rise for high fluences when the deposited energy is sufficient to heat the lower lying parts beyond the transition temperature T_T by heat diffusion. This unlocks a growth of the FM phase into the depth of the film. Modeling the UXRD results shows that this growth driven by near-equilibrium heat transport is considerably slower than the 8 ps nucleation timescale after heating above T_T, indicating the crucial role of optically induced non-thermal states for the kinetics of the phase transition. The heat transport timescale is cross-checked by a buried tungsten detection layer, which measures the energy transmitted through FeRh. To complement the insights from the structural order parameter, we probe the subsequent formation of a macroscopic out-of-plane magnetization within 180 ps by using polar tr-MOKE. When we excite the thick FeRh film from the backside, we find a considerably slower and fluence-dependent rise compared to frontside excitation, which experimentally verifies the slow out-of-plane growth of the FM phase.

The two samples are shown in Figs. 1(a) and 1(b) and consist of a 12.6 nm thick FeRh film on MgO(001) and a 43.8 nm thick FeRh film embedded in a metallic heterostructure on MgO(001) consisting of a 2 nm Pt capping and an 8 nm W buffer layer. The thickness of the layers has been characterized via x-ray reflectivity (XRR), and the FeRh films were grown using magnetron sputtering from an equiatomic FeRh target.[20] The W layer is purposely grown beneath the thick FeRh as an optically unexcited detection layer for the coherently excited strain pulses. Its strain response accesses the initial stress profile and calibrates the energy transport within the FeRh layer on longer timescales.[31] Both the FeRh films exhibit the first-order phase transition characterized by the temperature-dependent magnetization (solid lines) and average out-of-plane lattice constant d (symbols) shown in Figs. 1(c) and 1(d). They were measured in thermal equilibrium via vibrating sample magnetometry (VSM) using a QuantumDesign VersaLab magnetometer and XRD performed at the KMC-3 XPP endstation at BESSY II ,[32] respectively.

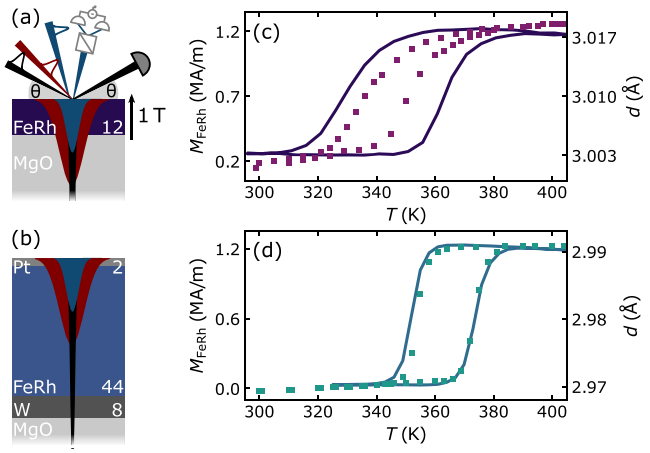

FIG. 1. Characterization of FeRh films: (a) and (b) sketch of the sample structures containing a 12 nm and a 44 nm FeRh film, the excitation profile (red) and the probing profile of UXRD (black) and MOKE (blue). The combined UXRD and MOKE experiment is sketched in panel (a). Panels (c) and (d) compare the temperature-dependent magnetization (solid lines) with the out-of-plane lattice constant (symbols) parametrizing the AFM-FM phase transition in the thin and thick FeRh film, respectively.

The thin film exhibits a reduced mean transition temperature of T_T = 365 K in comparison to the thick film (375 K) and a residual FM phase fraction of around 20% originating from interface effects.[33–35] This reduces the relative expansion associated with the AFM-FM phase transition from 0.6% in the thick film to 0.48% in the thin film. While the magnetization and lattice constant as order parameters of the temperature-induced phase transition nicely agree for the thick film, the inhomogeneity of the thin film results in a narrower hysteresis for the locally probed lattice constant in contrast to the global magnetization determined by VSM.

In the combined UXRD and tr-MOKE experiment, the FeRh layers are excited by p-polarized pump pulses with a central wavelength of 800 nm and 100 fs pulse duration that are incident under 50° with respect to the sample surface. Utilizing UXRD, we probe the transient out-of-plane strain response of the FeRh layers via reciprocal space mapping[36] of the FeRh(002) Bragg peak at a table-top laser-driven plasma x-ray source[37] providing 200 fs hard x-ray pulses with a photon energy of ≈8 keV. The Bragg peak position in reciprocal space is given by the average out-of-plane lattice constant d of the FeRh films via $q_z = 4\pi/d$. Therefore, the laser-induced peak shift accesses its change Δd determining the lattice strain $\eta_{FeRh} = \Delta d/d_0$ as the relative change with respect to its value d_0 before excitation.

Figure 2 shows the laser-induced strain response of both the FeRh films and the buried W layer to a weak sub-threshold excitation, which is not able to drive the AFM-FM phase transition.[27,28] Thus, the strain response is the superposition of only two contributions: a quasi-static expansion due to heating and coherently driven propagating strain pulses (partially) reflected at the surface and interfaces. In the nearly homogeneously excited 12 nm FeRh film, the laser excitation launches a strain pulse that is reflected at the surface and partially transmitted onto the substrate. This results in a decaying oscillation with a period of $2L_{FeRh}/v_s$ determined by the layer thickness L_{FeRh} and the sound velocity v_s[31] that is superimposed with a decreasing quasi-static expansion due to heat transport into the substrate [see Fig. 2(a)]. For the thick film sample, the bipolar strain pulse launched at the optically excited surface is partially reflected at the FeRh–W interface, which leads to a more complex shape of the oscillations in the FeRh strain response [see Fig. 2(b)]. The initial compression of the W layer is caused by the leading part of the bipolar strain pulse generated in FeRh and, hence essentially senses the energy profile.[31] The W strain turns positive when the expansive part of the strain pulse enters and the compressive part again exits the layer. The slowly rising expansion of W accesses the heat transport from FeRh into W on tens of picoseconds. These

thermoelastic strain contributions scale linearly with the deposited energy.[31]

In the following, we utilize this calibration of the thermoelastic strain response in the absence of a laser-induced AFM-FM phase transition to extract the transient FM volume fraction V_{FM} from the strain response to above-threshold excitations that additionally contains a strain signature from the forming FM phase. In order to subtract scaled noise-free sub-threshold data from the above-threshold measurements and in order to access the inhomogeneous spatiotemporal temperature profile within the 44 nm-thick FeRh film, we modeled the strain response by the modular PYTHON library UDKM1DSIM[38] utilizing literature values for the thermoelastic properties presented in Table S1. We calculate the absorption profile and solve the one-dimensional heat diffusion equation determining the spatiotemporal temperature that determines the stress on the lattice.[31] By solving the linear one-dimensional elastic wave equation for this stress, we finally calculate the strain response.[31] As an approximation, we use a simple one temperature model, which implies that electron-propagation within the electron–phonon coupling time[39] is negligible for the driving stress. Since the compression of W in the first 10 ps shown in Fig. 2(b) clearly indicates that the driving electron–phonon stress is still confined to about 13 nm, we consider this approximation useful. The supplementary material S1 describes the details of the strain modeling. Figures 2(c) and 2(d) show the spatiotemporal strain η and temperature increase ΔT for the incident fluence of F_{st} = 1.6 mJ/cm^2. Averaging the strain $\eta(z,t)$ over a respective layer yields the layer-specific strain response measured in our UXRD experiment. We find excellent agreement of the modeled strain response (solid lines) with the measurements in both samples. The excellent agreement with both the 44 nm FeRh and the buried W layer for a single set of parameters pinpoints the modeled spatiotemporal temperature shown in Fig. 2(c). The shape of the initial compression of W quantifies the absorption profile and its slowly rising expansion probes the heat propagated through the inhomogeneously excited FeRh layer.[31]

Figure 3(a) shows the strain response of the 12 nm-thin FeRh film for various fluences below and above the threshold of the phase transition. The dashed line denotes the modeled thermoelastic strain scaled to 1.8 mJ/cm^2, i.e., the hypothetical strain response without phase transition. The very large difference to the actual measurement (colored area) highlights the signature of the phase transition

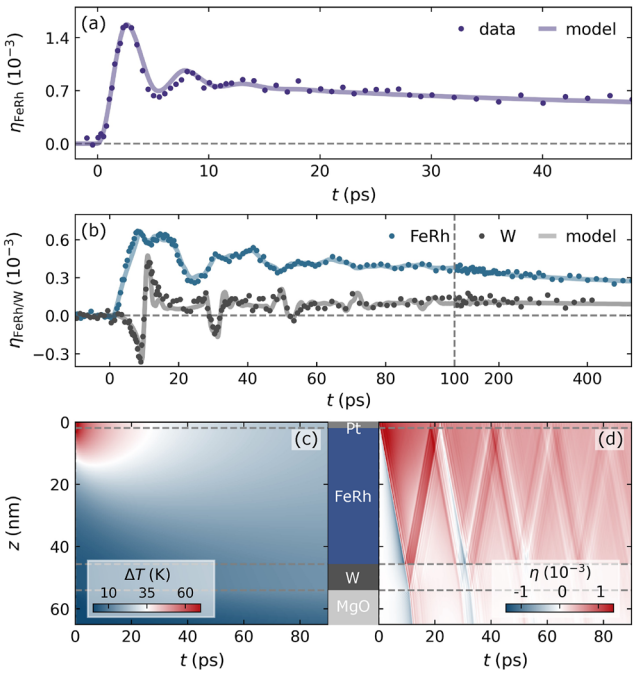

FIG. 2. Thermoelastic strain response calibrated by UXRD: (a) transient average strain of the 12 nm FeRh film (symbols) upon excitation with an incident fluence of F_{st} = 0.5 mJ/cm^2. (b) Transient average strain response of the 44 nm FeRh and the W layer (symbols) for F_{st} = 1.6 mJ/cm^2, which is sub-threshold (st) for the thick, Pt capped layer according to the tr-MOKE measurements shown in Fig. 4(c) The solid lines denote our strain model described in the text. The perfect agreement shown in panel (b) is strong evidence for the correct modeling of the corresponding spatiotemporal temperature increase $\Delta T(z,t)$ (c) and strain $\eta(z,t)$ (d).

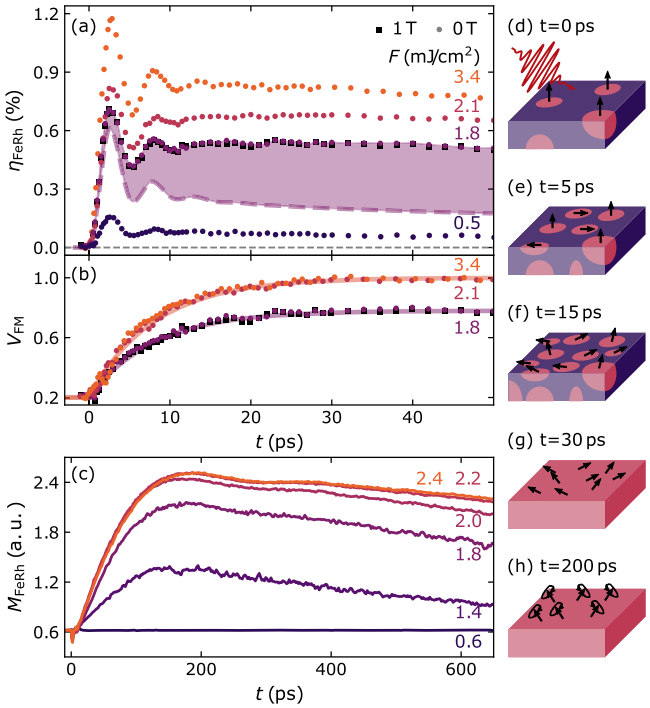

FIG. 3. Intrinsic timescale of nucleation: (a) fluence-dependent strain response of the 12 nm thick FeRh film. The strain response for a field of 1 T (squares) matches the one without external field (dots). The dashed line is the modeled strain for 0.5 mJ/cm^2 scaled to 1.8 mJ/cm^2, i.e., the hypothetical response without phase transition. (b) Transient FM volume fraction V_{FM} extracted from the difference (colored area) between the measurement and modeled thermoelastic strain. (c) Fluence-dependent transient out-of-plane magnetization from polar MOKE. Field-dependent MOKE data are shown in Fig. S4 in the supplementary material. Panels (d)–(h) sketch the kinetics of the phase transition in regard of the structural order parameter (pink color) and the magnetization (arrows) in line with the previous results.[14,28,29,42] After the nucleation of FM domains, the local magnetization precessionally tilts out-of-plane plane (g) and (h).

in the strain response. The strain measured in an external magnetic field of 1 T (squares) is identical to the response without an applied magnetic field (dots). This shows that the signature of the phase transition in the structural response is independent of the external magnetic field. We relate the additional strain contribution to the ferromagnetic volume fraction $V_{\mathrm{FM}}(t)$ by considering the expansion of 0.48% for a complete phase transition in thermal equilibrium [see Fig. 1(c)]. In addition, we considered the thermal expansion coefficient of the FM phase (see Table S1) and that the energy consumed by the latent heat 4.2 J/gK[40] at the transition temperature does not contribute to thermoelastic expansion. Figure 3(b) shows the extracted FM volume fraction $V_{\mathrm{FM}}(t)$ that parameterizes the laser-driven phase transition. We observe that $V_{\mathrm{FM}}(t)$ rises as a single exponential according to

$$V_{\mathrm{FM}}(t) = V_{\mathrm{FM}}^{*} \cdot \left(1 - e^{-t/\tau}\right), \tag{1}$$

where V_{FM}^{*} denotes the final fraction of the film in the FM phase and τ is the rise time, independent of the fluence and the applied magnetic field. This model of V_{FM} has been discussed and successfully applied in a previous UXRD study of FeRh[28] and assumes the nucleation of FM domains at independent sites according to the Avrami model.[1] We observe an intrinsic $\tau = 7.8 \pm 0.6$ ps timescale from the fit of all the measurements shown in Fig. 3(b). This is clearly slower than the relaxation of the lattice: the propagation of strain pulses through the thin film at the speed of sound only takes the time $L_{\mathrm{FeRh}}/v_s = 2.5$ ps [cf. Fig. 3(a)]. We can, therefore, definitely exclude the widely accepted hypothesis that the sound velocity v_s sets the speed limit for the AFM-FM phase transition in FeRh.[28,29,41] Instead, the structural order parameter intrinsically responds on an 8 ps timescale to direct optical excitation. The transformed volume fraction V_{FM}^{*} increases with fluence and saturates at $F_{\mathrm{sat}} = 2.1$ mJ/cm^2 when the complete film is driven into the FM phase. Figure 3(b) shows that $F = 3.4$ mJ/cm^2 yields the same V_{FM}^{*}, although the thermoelastic strain contributions grow [Fig. 3(a)]. We note that the stress on the lattice associated with the phase transition barely drives any propagating strain pulses because it rises much more slowly than the strain relaxes across the excited thickness within 2.5 ps at the speed of sound. This makes our method to subtract scaled sub-threshold data so efficient.

We complement the insights of the UXRD measurements by measuring the transient out-of-plane magnetization by polar MOKE in the very same experimental setup under identical excitation conditions. We applied a maximum out-of-plane magnetic field of 1 T provided by an electromagnet. The transient magnetization is extracted by the difference of the transient MOKE signal for opposite field-polarities. The 100 fs-long p-polarized probe pulse with a central wavelength of 400 nm is focused through the pole of the magnet and is incident under less than 2° with respect to the sample normal.

The transient out-of-plane magnetization shown in Fig. 3(c) verifies this fluence dependence of V_{FM}^{*}. Up to the threshold fluence of $F_{\mathrm{th}} = 0.6$ mJ/cm^2, we observe no macroscopic magnetization at all and a fluence of 2.1 mJ/cm^2 fully saturates the laser-induced magnetization. We observe a fluence-independent rise time with the maximum signal at 180 ps for 1 T, i.e., much slower than the nucleation of the FM domains. This slow formation of a macroscopic magnetization by the alignment of the local magnetization of the nucleated domains was reported previously.[27–29] The local magnetization initially lies in the sample plane along four equal directions determined by a cubic anisotropy of around 100 mT that represent the magnetic easy axes due to the shape anisotropy field of 1.38 T for thin FeRh films.[28,43] For an in-plane magnetic field, a macroscopic in-plane magnetization is formed by field-driven coalescence of the FM domains via domain wall motion in agreement with the observed linear increase in the growth rate of the macroscopic magnetization with the field.[29] In contrast, for the out-of-plane magnetization, we observe the maximum to be established faster for smaller out-of-plane fields (Fig. S4). This is consistent with precessionally tilting[14] the magnetization of the nucleated domains out of the sample plane. Figures 3(d)–3(h) show the series of events.

These MOKE results upon direct optical excitation of the thin film serve as a reference for the inhomogeneously excited thick film where the redistribution of energy within the layer by heat transport extends the dynamics of the phase transition. We utilize the finite probing depth of MOKE to gain insights into the out-of-plane evolution of the FM phase by comparing the rising magnetization at the sample surface for front- and backside excitation shown in Figs. 4(c) and 4(d). For frontside excitation, we observe the same fluence-independent rise time as for the thin film shown in Fig. 3(c). In contrast, exciting through the substrate leads to a delayed and slower rise. In addition, the rise time strongly depends on the fluence (see Fig. S3 for a comparison normalized to the maximum). The delayed and much slower rise for backside excitation is fluence-dependent, indicating a slow out-of-plane growth of V_{FM} via near-equilibrium heat transport that brings the upper part of the film above the transition temperature. However, the tr-MOKE measurements cannot quantify whether it is the heat transport or different kinetics of the phase transition in near-equilibrium that yield the increased timescale.

In order to determine the speed at which the FM phase nucleates and grows in the thick film, we again subtract the fluence-scaled strain response to a sub-threshold excitation F_{st} shown in Fig. 4(a) measured by UXRD from the strain measured above the threshold. The resulting transient FM volume fraction in Fig. 4(b) shows the change from a single exponential rise for low fluences to a two-step rise for high fluences (>6 mJ/cm^2). For all fluences, V_{FM} rises according to Eq. (1) with the intrinsic 8 ps timescale already observed in the thin film during the first 30 ps [see the solid colored lines shown in Fig. 4(b)]. The amplitude of the additional contribution in the high fluence regime increases with the fluence. The maximum V_{FM} is reached at increasing delays up to 250 ps for the highest fluence, where the complete FeRh film is driven across the AFM-FM phase transition. Reaching the full transformation to the FM phase in Fig. 4(b) shows that for high fluences, the temperature at the backside finally exceeds the transition temperature T_{T}, thus enabling the phase transition in near-equilibrium. This results in the two-step rise of V_{FM} for high fluences in contrast to a phase transition on the 8 ps timescale limited to the optically excited near-surface region for low fluences, as shown in Figs. 4(e)–4(h). Note that the laterally homogeneous growth of the FM phase into the depth, which follows the inhomogeneous optical excitation, differs from the dynamics observed for homogeneous equilibrium heating,[2] where columns through the FeRh film are formed after the nucleation of FM domains at both interfaces before the in-plane domain growth.

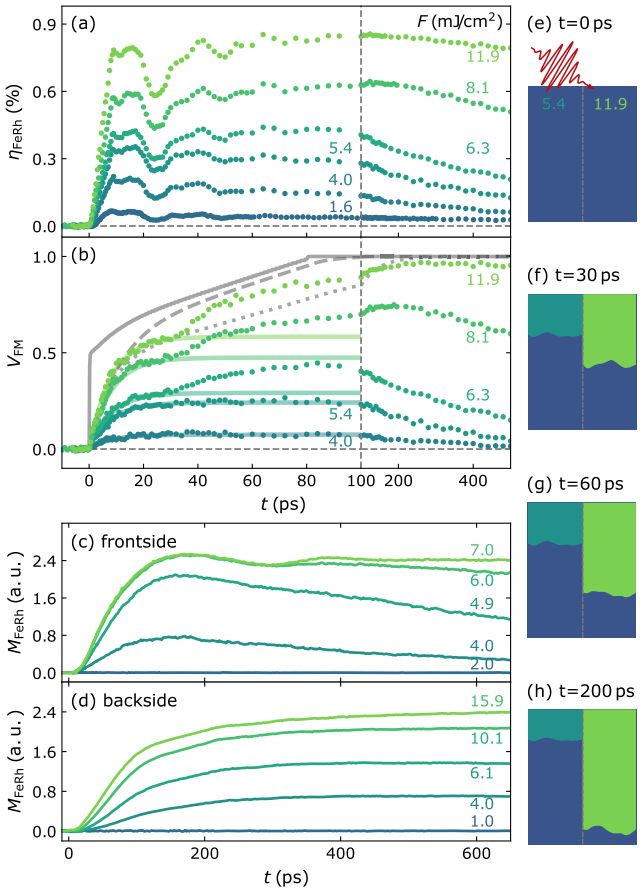

FIG. 4. Kinetics of out-of-plane growth of the FM phase: (a) fluence-dependent field-free strain response of the 44 nm thick FeRh film. (b) Transient FM volume fraction derived analogously to the thin film by comparing the measured strain to a scaled sub-threshold strain model. (c) and (d) Fluence-dependent magnetization rise measured by polar MOKE with a magnetic field of 1 T in frontside and backside excitation geometry, respectively. (e)–(h) Sketch of the out-of-plane growth of the FM phase indicated by the green area for 5.4 (left) and 11.9 mJ/cm^2 (right) that is induced by fluence-dependent heating above T_T at the backside of the film via near-equilibrium heat transport.

To cross-check our interpretation, we repeated the UXRD varying the initial sample temperature (cf. Fig. S2). At temperatures only slightly below T_T, the laser excitation is sufficient to drive the phase transition in the not directly excited bottom part of FeRh, which results in a two-step rise of V_{FM}. At lower temperatures, the heating is insufficient and we observe only a rise on the 8 ps timescale. In this temperature-dependent experiment, we directly accessed V_{FM} by the transient relative amplitudes of the structural Bragg peaks of the AFM and FM phases that are separated in a reciprocal space due to the excellent collimation of the x-ray beam at the KMC-3 XPP endstation at BESSY II.[32] This parameter-free analysis also applied by Mariager and co-workers[28] serves as a cross-check of our findings shown in Figs. 3 and 4. The slow growth of the FM phase into the depth unlocked by strong excitations explains the different timescales for different fluences and probing depth reported in previous UXRD experiments on inhomogeneously excited FeRh films.[28,30] The exponential probing profile in grazing incidence geometry[28] may have masked the clear two-step behavior observed in our experiments.

We obtain additional insights into the growth of the FM phase within the inhomogeneously excited FeRh layer from the modeled spatiotemporal temperature profile $T(z,t)$ shown in Fig. 2(c). From this analysis, we obtain the gray solid line shown in Fig. 4(b), which denotes the fraction of the film transiently heated above T_T = 375 K for an excitation of 11.9 mJ/cm^2. We explicitly take into account the required additional energy that is consumed by the latent heat of the phase transition, which would otherwise raise the lattice temperature by about 8 K for the full transition. This analysis shows that already within the first 30 ps a considerably large fraction and, within 80 ps, the complete film is heated above the transition temperature. This is much faster than the observed rise of V_{FM} within 250 ps and indicates that the growth of the FM phase does not simply follow the heating of the backside above T_T but exhibits intrinsic kinetics. If we assume the FM phase to locally rise with an 8 ps timescale as soon as the local temperature exceeds T_T, the modeled rise of V_{FM} (gray dashed line) is still significantly faster than in the measurement. Therefore, establishing the FM phase by only near-equilibrium heating must be considerably slower than the nucleation in the optically excited near-surface part of the film. The gray dotted line shown in Fig. 4(b) represents the combination of an 8 ps nucleation timescale for the optically heated unit cells and a second 50 ps timescale for the formation of the FM phase for unit cells heated above T_T by heat transport. This approach matches the delay when V^*_{FM} is reached and provides an estimation of the intrinsic timescale related to the phase transition driven by near-equilibrium heating via thermal electrons and phonons. The deviation of our simple model from the experiment between 40 and 80 ps may originate from a more complex heat transport within FeRh due to the large latent heat of the phase transition[44] and an interplay of the locally rising FM phase upon direct photo-excitation and near-equilibrium heating.

In summary, we discovered an intrinsic fluence-, temperature-, and field-independent 8 ps timescale for locally establishing macroscopic properties of the FM phase in FeRh via the nucleation of domains upon direct optical excitation. This timescale is not limited by the relaxation of the lattice with sound velocity as stated previously[28,41] but represents intrinsic kinetics of the first-order phase transition. Previous photoemission spectroscopy experiments reported a change in the electronic band structure within the first picosecond upon laser excitation.[25] In the vicinity of a thick Cu layer serving as a spin bath, Kang and co-workers[41] recently observed a fast rise in the magnetization of FeRh within the first picoseconds in contrast to the previously reported latency in the formation of a macroscopic magnetization.[28,29] This hints that the fast dynamics observed by Kang and co-workers may be related to the spin transport into the thick Cu layer after the ultrafast formation of the intermediate non-equilibrium state of FeRh indicated by the change in the electronic band structure. However, in our experiments, we only probe the subsequent formation of the equilibrium FM phase via the nucleation of domains. In addition to the photo-induced nucleation of FM domains in the near-surface region, we observe

a slow growth of the FM phase into the depth of an inhomogenously excited FeRh layer driven by near-equilibrium heat transport in case of high fluences and sample temperatures near the transition temperature. This additional slow contribution enabled by high fluences explains the different rise times of the structural order parameter in previous UXRD experiments[28,30] and clarifies the timescale of the formation of a local equilibrium FM phase. Our modeling reveals that the FM phase rises approximately on a 50 ps timescale after heating above the transition temperature by near-equilibrium heat transport, which is substantially slower than the nucleation upon direct optical excitation in the near-surface region. This hints to the crucial role of modifying the electronic band structure within the first picosecond via photoexcited electrons[25] for the kinetics of the subsequent formation of the equilibrium FM phase.

SUPPLEMENTARY MATERIAL

The supplementary material contains a detailed description for modeling the thermoelastic strain response, including all parameters. Additional temperature dependent UXRD data reconfirm conclusions drawn from the fluence dependence shown in Fig. 4. MOKE measurements for varied external magnetic field are presented.

ACKNOWLEDGMENTS

We acknowledge the DFG for financial support via Grant No. BA 2281/11-1 and Project-No. 328545488 – TRR 227, Project No. A10. V. U. acknowledges Project No. CZ.02.01.01/00/22_008/0004594. Access to the CzechNanoLab Research Infrastructure was supported by the MEYS CR (Grant No. LM2023051). Beamtimes at the KMC-3 XPP endstation of the synchrotron radiation facility BESSY II at the Helmholtz Zentrum Berlin were required for thorough sample characterization and parameter-free crosscheck measurements. Open access funding is provided by the Deutsche Forschungsgemeinschaft (DFG, German Research Foundation) – Projektnummer 491466077.

AUTHOR DECLARATIONS

Conflict of Interest

The authors have no conflicts to disclose.

Author Contributions

M. Mattern: Conceptualization (equal); Data curation (lead); Formal analysis (lead); Investigation (lead); Methodology (equal); Software (equal); Validation (equal); Visualization (lead); Writing – original draft (lead); Writing – review & editing (equal). **J. Jarecki**: Investigation (supporting); Writing – original draft (supporting). **J. A. Arregi**: Investigation (equal); Methodology (equal); Resources (equal); Writing – original draft (supporting); Writing – review & editing (supporting). **V. Uhlíř**: Funding acquisition (equal); Resources (equal); Supervision (equal); Validation (equal); Writing – original draft (supporting); Writing – review & editing (supporting). **M. Rössle**: Data curation (equal); Investigation (equal); Methodology (equal); Writing – original draft (supporting); Writing – review & editing (supporting). **M. Bargheer**: Conceptualization (equal); Funding acquisition (equal); Investigation (equal); Methodology (lead); Project administration (lead); Resources (lead); Supervision (lead); Validation (equal); Writing – original draft (equal); Writing – review & editing (equal).

DATA AVAILABILITY

The data that support the findings of this study are available from the corresponding author upon reasonable request.

REFERENCES

[1] M. Avrami, "Kinetics of phase change. I. General theory," J. Chem. Phys. **7**, 1103 (1939).
[2] C. Gatel, B. Warot-Fonrose, N. Biziere, L. Rodríguez, D. Reyes, R. Cours, M. Castiella, and M.-J. Casanove, "Inhomogeneous spatial distribution of the magnetic transition in an iron-rhodium thin film," Nat. Commun. **8**, 15703 (2017).
[3] V. Uhlíř, J. A. Arregi, and E. E. Fullerton, "Colossal magnetic phase transition asymmetry in mesoscale FeRh stripes," Nat. Commun. **7**, 13113 (2016).
[4] J. A. Arregi, F. Ringe, J. Hajduček, O. Gomonay, T. Molnár, J. Jaskowiec, and V. Uhlíř, "Magnetic-field-controlled growth of magnetoelastic phase domains in FeRh," J. Phys.: Mater. **6**, 034003 (2023).
[5] S. Roy, G. Perkins, M. Chattopadhyay, A. Nigam, K. Sokhey, P. Chaddah, A. Caplin, and L. Cohen, "First order magnetic transition in doped $CeFe_2$ alloys: Phase coexistence and metastability," Phys. Rev. Lett. **92**, 147203 (2004).
[6] S. De Jong, R. Kukreja, C. Trabant, N. Pontius, C. Chang, T. Kachel, M. Beye, F. Sorgenfrei, C. Back, B. Bräuer *et al.*, "Speed limit of the insulator–metal transition in magnetite," Nat. Mater. **12**, 882 (2013).
[7] F. Randi, I. Vergara, F. Novelli, M. Esposito, M. Dell'Angela, V. Brabers, P. Metcalf, R. Kukreja, H. A. Dürr, D. Fausti *et al.*, "Phase separation in the nonequilibrium Verwey transition in magnetite," Phys. Rev. B **93**, 054305 (2016).
[8] M. M. Qazilbash, M. Brehm, B.-G. Chae, P.-C. Ho, G. O. Andreev, B.-J. Kim, S. J. Yun, A. Balatsky, M. Maple, F. Keilmann *et al.*, "Mott transition in VO_2 revealed by infrared spectroscopy and nano-imaging," Science **318**, 1750 (2007).
[9] C. Baldasseroni, C. Bordel, A. Gray, A. Kaiser, F. Kronast, J. Herrero-Albillos, C. Schneider, C. Fadley, and F. Hellman, "Temperature-driven nucleation of ferromagnetic domains in FeRh thin films," Appl. Phys. Lett. **100**, 262401 (2012).
[10] D. J. Keavney, Y. Choi, M. V. Holt, V. Uhlíř, D. Arena, E. E. Fullerton, P. J. Ryan, and J.-W. Kim, "Phase coexistence and kinetic arrest in the magnetostructural transition of the ordered alloy FeRh," Sci. Rep. **8**, 1778 (2018).
[11] S. Polesya, S. Mankovsky, D. Ködderitzsch, J. Minár, and H. Ebert, "Finite-temperature magnetism of FeRh compounds," Phys. Rev. B **93**, 024423 (2016).
[12] D. Wegkamp, M. Herzog, L. Xian, M. Gatti, P. Cudazzo, C. L. McGahan, R. E. Marvel, R. F. Haglund, Jr., A. Rubio, M. Wolf, and J. Stähler, "Instantaneous band gap collapse in photoexcited monoclinic VO_2 due to photocarrier doping," Phys. Rev. Lett. **113**, 216401 (2014).
[13] G. Ju, J. Hohlfeld, B. Bergman, R. J. van de Veerdonk, O. N. Mryasov, J.-Y. Kim, X. Wu, D. Weller, and B. Koopmans, "Ultrafast generation of ferromagnetic order via a laser-induced phase transformation in FeRh thin films," Phys. Rev. Lett. **93**, 197403 (2004).
[14] B. Bergman, G. Ju, J. Hohlfeld, R. J. van de Veerdonk, J.-Y. Kim, X. Wu, D. Weller, and B. Koopmans, "Identifying growth mechanisms for laser-induced magnetization in FeRh," Phys. Rev. B **73**, 060407 (2006).
[15] E. Beaurepaire, J.-C. Merle, A. Daunois, and J.-Y. Bigot, "Ultrafast spin dynamics in ferromagnetic nickel," Ultrafast Phenom. **76**, 4250 (1996).
[16] A. Kirilyuk, A. V. Kimel, and T. Rasing, "Ultrafast optical manipulation of magnetic order," Rev. Mod. Phys. **82**, 2731 (2010).
[17] C. D. Stanciu, F. Hansteen, A. V. Kimel, A. Kirilyuk, A. Tsukamoto, A. Itoh, and T. Rasing, "All-optical magnetic recording with circularly polarized light," Phys. Rev. Lett. **99**, 047601 (2007).
[18] I. Radu, K. Vahaplar, C. Stamm, T. Kachel, N. Pontius, H. Dürr, T. Ostler, J. Barker, R. Evans, R. Chantrell *et al.*, "Transient ferromagnetic-like state mediating ultrafast reversal of antiferromagnetically coupled spins," Nature **472**, 205 (2011).

[19]Q. Remy, J. Hohlfeld, M. Vergès, Y. Le Guen, J. Gorchon, G. Malinowski, S. Mangin, and M. Hehn, "Accelerating ultrafast magnetization reversal by non-local spin transfer," Nat. Commun. **14**, 445 (2023).
[20]J. A. Arregi, O. Caha, and V. Uhlíř, "Evolution of strain across the magnetostructural phase transition in epitaxial FeRh films on different substrates," Phys. Rev. B **101**, 174413 (2020).
[21]A. Gray, D. Cooke, P. Krüger, C. Bordel, A. Kaiser, S. Moyerman, E. Fullerton, S. Ueda, Y. Yamashita, A. Gloskovskii *et al.*, "Electronic structure changes across the metamagnetic transition in FeRh via hard x-ray photoemission," Phys. Rev. Lett. **108**, 257208 (2012).
[22]F. Pressacco, V. Uhlíř, M. Gatti, A. Nicolaou, A. Bendounan, J. A. Arregi, S. K. Patel, E. E. Fullerton, D. Krizmancic, and F. Sirotti, "Laser induced phase transition in epitaxial FeRh layers studied by pump-probe valence band photoemission," Struct. Dyn. **5**, 034501 (2018).
[23]S. Maat, J.-U. Thiele, and E. E. Fullerton, "Temperature and field hysteresis of the antiferromagnetic-to-ferromagnetic phase transition in epitaxial FeRh films," Phys. Rev. B **72**, 214432 (2005).
[24]C. Stamm, J.-U. Thiele, T. Kachel, I. Radu, P. Ramm, M. Kosuth, J. Minár, H. Ebert, H. Dürr, W. Eberhardt, and C. H. Back, "Antiferromagnetic-ferromagnetic phase transition in FeRh probed by x-ray magnetic circular dichroism," Phys. Rev. B **77**, 184401 (2008).
[25]F. Pressacco, D. Sangalli, V. Uhlíř, D. Kutnyakhov, J. A. Arregi, S. Y. Agustsson, G. Brenner, H. Redlin, M. Heber, D. Vasilyev *et al.*, "Subpicosecond metamagnetic phase transition in FeRh driven by non-equilibrium electron dynamics," Nat. Commun. **12**, 5088 (2021).
[26]A. Ünal, A. Parabas, A. Arora, J. Ehrler, C. Barton, S. Valencia, R. Bali, T. Thomson, F. Yildiz, and F. Kronast, "Laser-driven formation of transient local ferromagnetism in FeRh thin films," Ultramicroscopy **183**, 104 (2017).
[27]I. Radu, C. Stamm, N. Pontius, T. Kachel, P. Ramm, J.-U. Thiele, H. Dürr, and C. Back, "Laser-induced generation and quenching of magnetization on FeRh studied with time-resolved x-ray magnetic circular dichroism," Phys. Rev. B **81**, 104415 (2010).
[28]S. O. Mariager, F. Pressacco, G. Ingold, A. Caviezel, E. Möhr-Vorobeva, P. Beaud, S. Johnson, C. Milne, E. Mancini, S. Moyerman *et al.*, "Structural and magnetic dynamics of a laser induced phase transition in FeRh," Phys. Rev. Lett. **108**, 087201 (2012).
[29]G. Li, R. Medapalli, J. Mentink, R. Mikhaylovskiy, T. Blank, S. Patel, A. Zvezdin, T. Rasing, E. Fullerton, and A. Kimel, "Ultrafast kinetics of the antiferromagnetic-ferromagnetic phase transition in FeRh," Nat. Commun. **13**, 2998 (2022).
[30]F. Quirin, M. Vattilana, U. Shymanovich, A.-E. El-Kamhawy, A. Tarasevitch, J. Hohlfeld, D. von der Linde, and K. Sokolowski-Tinten, "Structural dynamics in FeRh during a laser-induced metamagnetic phase transition," Phys. Rev. B **85**, 020103 (2012).
[31]M. Mattern, A. von Reppert, S. P. Zeuschner, M. Herzog, J.-E. Pudell, and M. Bargheer, "Concepts and use cases for picosecond ultrasonics with x-rays," Photoacoustics **31**, 100503 (2023).
[32]M. Rössle, W. Leitenberger, M. Reinhardt, A. Koç, J. Pudell, C. Kwamen, and M. Bargheer, "The time-resolved hard X-ray diffraction endstation KMC-3 XPP at BESSYII," J. Synchrotron Radiat. **28**, 948 (2021).
[33]F. Pressacco, V. Uhlíř, M. Gatti, A. Bendounan, E. E. Fullerton, and F. Sirotti, "Stable room-temperature ferromagnetic phase at the FeRh(100) surface," Sci. Rep. **6**, 22383 (2016).
[34]R. Fan, C. J. Kinane, T. Charlton, R. Dorner, M. Ali, M. De Vries, R. M. Brydson, C. H. Marrows, B. J. Hickey, D. A. Arena *et al.*, "Ferromagnetism at the interfaces of antiferromagnetic FeRh epilayers," Phys. Rev. B **82**, 184418 (2010).
[35]X. Chen, J. Feng, Z. Wang, J. Zhang, X. Zhong, C. Song, L. Jin, B. Zhang, F. Li, M. Jiang *et al.*, "Tunneling anisotropic magnetoresistance driven by magnetic phase transition," Nat. Commun. **8**, 449 (2017).
[36]D. Schick, R. Shayduk, A. Bojahr, M. Herzog, C. von Korff Schmising, P. Gaal, and M. Bargheer, "Ultrafast reciprocal-space mapping with a convergent beam," J. Appl. Crystallogr. **46**, 1372 (2013).
[37]D. Schick, A. Bojahr, M. Herzog, C. v. K. Schmising, R. Shayduk, W. Leitenberger, P. Gaal, and M. Bargheer, "Normalization schemes for ultrafast x-ray diffraction using a table-top laser-driven plasma source," Rev. Sci. Instrum. **83**, 025104 (2012).
[38]D. Schick, "udkm1Dsim—A Python toolbox for simulating 1D ultrafast dynamics in condensed matter," Comput. Phys. Commun. **266**, 108031 (2021).
[39]S. Günther, C. Spezzani, R. Ciprian, C. Grazioli, B. Ressel, M. Coreno, L. Poletto, P. Miotti, M. Sacchi, G. Panaccione *et al.*, "Testing spin-flip scattering as a possible mechanism of ultrafast demagnetization in ordered magnetic alloys," Phys. Rev. B **90**, 180407 (2014).
[40]M. Richardson, D. Melville, and J. Ricodeau, "Specific heat measurements on an Fe Rh alloy," Phys. Lett. A **46**, 153 (1973).
[41]K. Kang, H. Omura, D. Yesudas, O. Lee, K.-J. Lee, H.-W. Lee, T. Taniyama, and G.-M. Choi, "Spin current driven by ultrafast magnetization of FeRh," Nat. Commun. **14**, 3619 (2023).
[42]N. Agarwal, "Ultrafast dynamics of electronic structure and domain nucleation during photo-induced phase transition in FeRh," Ph.D. thesis, Staats-und Universitätsbibliothek Hamburg Carl von Ossietzky 2021.
[43]J. Cao, N. T. Nam, S. Inoue, H. Y. Y. Ko, N. N. Phuoc, and T. Suzuki, "Magnetization behaviors for FeRh single crystal thin films," J. Appl. Phys. **103**, 07F501 (2008).
[44]Y. Ahn, M. J. Cherukara, Z. Cai, M. Bartlein, T. Zhou, A. DiChiara, D. A. Walko, M. Holt, E. E. Fullerton, P. G. Evans, and H. Wen, "X-ray nanodiffraction imaging reveals distinct nanoscopic dynamics of an ultrafast phase transition," Proc. Natl. Acad. Sci. U. S. A. **119**, e2118597119 (2022).